Carbon-Nanotube-Induced Acceleration of Catalytic Nanomotors

Rawiwan Laocharoensuk, Jared Burdick, and Joseph Wang*

Biodesign Institute, Departments of Chemical Engineering and Chemistry and Biochemistry, Arizona State University, Tempe, Arizona 85287

ABSTRACT Synthetic nanoscale motors represent a major step toward the development of practical nanomachines. Despite impressive progress, man-made nanomachines lack the efficiency and speed of their biological counterparts. Here we show that the incorporation of carbon nanotubes (CNT) into the platinum (Pt) component of asymmetric metal nanowire motors leads to dramatically accelerated movement in hydrogen-peroxide solutions, with average speeds (50−60 μm/s) approaching those of natural biomolecular motors. Further acceleration—to 94 μm/s, with some motors moving above 200 μm/s—is observed upon adding hydrazine to the peroxide fuel. Factors influencing the accelerated movement, including the CNT loading and fuel concentration, are examined. Such development of highly efficient and controllable nanomotors offers great promise for self-powered nanoscale transport and delivery systems.

KEYWORDS: carbon nanotubes · catalytic nanomotors · high speed · hydrogen peroxide · hydrazine

Nanoscale biomolecular motors, based on spontaneous reactions of energy-rich molecules (*e.g.*, adenosine triphosphate (ATP)), are common in nature.[1−3] Such mechanical function of biomolecules provides an inspiration for the development of man-made nanomachines, operating on locally supplied fuels and performing various tasks ranging from drug delivery to moving cargo in microfluidic devices.[1,2] Recent efforts toward the design of synthetic motors have demonstrated the ability to convert chemical energy into autonomous motion.[4−7] In particular, several groups have developed self-powered Au/Pt or Au/Ni bimetal nanowire motors based on the catalytic decomposition of hydrogen peroxide fuel to oxygen and water.[5−7] Such electrochemically grown nanowires display autonomous movement in the axial direction with speeds of around 10 μm/s.[5] Despite this remarkable progress the efficiency, speed, and versatility of synthetic nanomachines pale in comparison to their natural counterparts leaving much room for improvement.

Here we demonstrate that the incorporation of carbon nanotubes (CNT) within the Pt segment of catalytic nanowires, along with the addition of hydrazine to the peroxide fuel, leads to a dramatic acceleration of their movement. The resulting Au/Pt−CNT nanowires display high average speeds of *ca.* 94 μm/s, with some wires traveling at speeds faster than 200 μm/s (equivalent to 100 body-lengths/second), hence surpassing the speeds of most biological motors. The ultrafast motion of Au/Pt−CNT nanowires reflects the enhanced catalytic decomposition of the peroxide fuel on the Pt−CNT end. CNT were used before by Zettl's group as support shafts for rotational actuators[8] and as nanoscale mass conveyors[9] but not in connection to catalytic nanomotors. We expect that the development of highly efficient and controllable nanomotors will open the door to powerful nanovehicle systems performing diverse operations of increasing complexity.

RESULTS AND DISCUSSION

Figure 1 shows the influence of the CNT incorporation (into the Pt segment) upon the speed of the Au/Pt nanomotors. The top insets show traces of three Au/Pt (a) and Au/Pt−CNT (b) nanomotors, taken from videos of the nanowires in the presence of 15 wt % aqueous H_2O_2 fuel over a 4 s period. The Au/Pt−CNT nanowires travel substantially longer distances (>7-fold) over the same time period (average distance of 204 μm *vs* 29 μm for the Au/Pt wires), indicating a substantial speed acceleration associated with the presence of CNT in the Pt segment. Examples of the videos used for recording the movement of both types of nanomotors (video 1) are provided with Figure 1 in the Web version of this article. The motion of both nanomotors is direc-

Ⓦ This paper contains enhanced objects available on the Internet at http://pubs.acs.org/journals/ancac3.

*Address correspondence to joseph.wang@asu.edu.

Received for review March 14, 2008 and accepted April 09, 2008.

Published online April 24, 2008.
10.1021/nn800154g CCC: $40.75

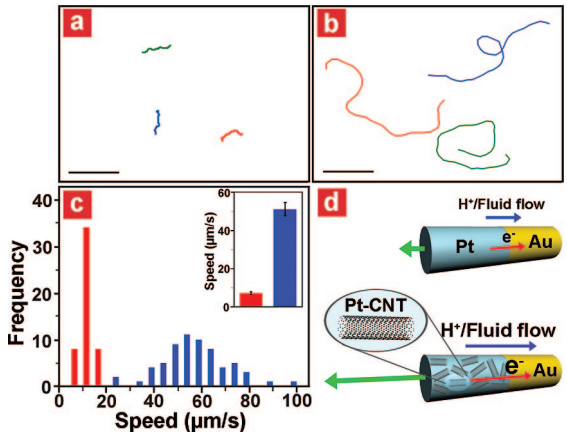

Figure 1. CNT-induced high speed catalytic nanomotors: (a, b) Tracking lines illustrating a typical motion and moving distances of Au/Pt (a) and Au/Pt−CNT (0.50 mg/ml) (b) nanomotors during a period of 4 s in the presence of 15 wt % hydrogen peroxide fuel. Scale bar is 45 μm. (c) Histograms of average speeds of Au/Pt (red) and Au/Pt−CNT (blue) nanomotors measured from the movement of the nanomotors in a 15 wt % hydrogen-peroxide fuel over a 10 s period. Bar graphs with *Y* error bars (inset) represent the mean of average speeds (μm/s) and the error limit at 90% confidence interval of the corresponding nanomotors, respectively. (d) A schematic representation of the self-electrophoresis mechanism of Au/Pt (top) and Au/Pt−CNT (bottom) bipolar nanomotors. Hydrogen peroxide fuel is preferentially consumed/oxidized on the Pt (top, blue) or Pt−CNT (bottom, patterned blue) ends while oxygen is catalytically reduced on the Au (yellow) segment. The flux of electrons inside the nanomotors proceeds from one end to the other generating a local electric field, as well as the migration of protons and surrounding fluid outside the nanomotors resulting in the movement of the nanomotor in the opposite direction. The higher electrocatalytic activity of Pt−CNT compared with Pt provides a faster reaction rate, and hence a higher proton and fluid flow corresponding to an increased flux of electrons inside the nanomotors as indicated by the vectors.

Ⓦ video 1, showing the typical motion of nanomotors is available.

tional with the Pt or Pt−CNT side forward. Figure 1c shows a histogram representation of the speed distribution of both the Au/Pt (red) and Au/Pt−CNT (blue) nanowires. A nearly Gaussian speed distribution is observed for both motors ($n \geq 50$). Average speeds of 7.2 μm/s (Au/Pt) and 51.0 μm/s (Au/Pt−CNT) are indicated from the inset bar graph in the histogram plots (c). The former is in good agreement with the literature value of 7.7 μm/s reported by Paxton *et al.*[5] As will be illustrated below, changing the fuel composition, particularly adding a second component (hydrazine) to the peroxide solution, greatly increases the average speed of the Au/Pt−CNT nanowires to over 94 μm/s. The lifetime of the nanomotors in the aqueous H_2O_2 solution (at the concentration shown in video 1) is greater than half an hour. During this period the nanomotors continue their movement without deceleration, traveling distances greater than 10 cm.

The ratio of chemical power input (fuel consumption) to mechanical power output defines the energy conversion efficiency of the catalytic engine. The chemical power input is realized by determining the rate of the hydrogen peroxide decomposition times the free energy of the reaction. This decomposition rate can be determined by measuring the oxygen generation rate[10] or by measuring the electron transfer rate on the catalytic end in hydrogen peroxide fuel. The relative input power can then be calculated by the multiplying of the electron transfer rate with the free energy of the reaction. For a moving object in a surrounding liquid, the output power is the product of drag force overcome (Stokes's drag) and the velocity of the object. Based on these considerations, the energy conversion of Au/Pt−CNT nanomotors is over 8 times more efficient than that of Au/Pt nanomotors in 5 wt % H_2O_2 fuel.

Figure 1d displays a schematic representation of the Au/Pt and Au/Pt−CNT nanomotors, indicating the enhanced electron transfer and speed vectors associated with the presence of CNT in the Pt segment. The self-electrophoresis mechanism, proposed by Paxton *et al.*,[10] gives good approximation of the axial autonomous movement of Au/Pt bimetallic nanomotors moving with the Pt side first. This mechanism considers that the oxidation of H_2O_2 occurs preferentially on the Pt end while the reduction of both H_2O_2 and O_2 takes place on the Au side. When the nanomotors are immersed in the aqueous H_2O_2 fuel solution these simultaneous reactions cause the nanomotors to act as galvanic cells with electrons transferring inside the nanomotors from the Pt (anodic) end to the Au (cathodic) end. Such internal flux of electrons is compensated by an equal and opposite external flux of protons in the electrical double layer (EDL) surrounding the rods. This proton flux "pushes" against the fluid and leads to directional motion of the nanomotors. The speed and direction of the movement of nanomotors are strongly dependent upon the potential of the galvanic reaction.[11] Metal pairs that have greater potential differences (due to redox reactions in the peroxide fuel) create a larger flux of electrons and hence a faster nanomotor speed.

CNT are well recognized for their attractive mechanical and electronic properties.[12] Various CNT-modified electrodes, displaying enhanced electrocatalytic activity, have benefited various sensing and energy applications.[13] Accelerated electron-transfer reactions and lower overvoltages have thus been demonstrated for several important molecules, including hydrogen peroxide.[14] The coupling of CNT with Pt surfaces has led to further improvements in the electron-transfer processes of hydrogen peroxide and oxygen in connection to various biosensing[15] and fuel-cell[16] applications. The primary reason for the enhanced electrochemical reactivity of CNT is not fully clear and appears to reflect edge-plane effects,[17] as well as contributions of peroxidase-like metal impurities (*e.g.*, Fe_2O_3, Fe_3O_4).[18] Although it is known that CNT aid in both the oxidation of H_2O_2[14] and reduction of O_2[19] it will be illustrated

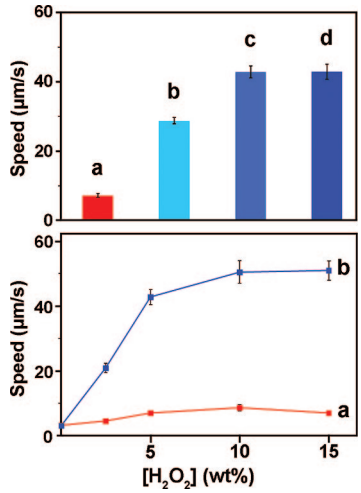

Figure 2. Effect of the CNT loading (top) and of the hydrogen peroxide fuel concentration (bottom) upon the speed of catalytic nanomotors. (Top) Bar graphs comparing the average speed of Au/Pt−CNT nanomotors (in 5 wt % hydrogen peroxide) as a function of the CNT loading: 0 (a), 0.25 (b), 0.50 (c), and 1.00 (d) mg/ml in the Pt-plating solution. The average speed of the Au/Pt (red bar) nanomotor was used as a standard value. *Y* error bars show the error limit at a 90% confidence interval. (Bottom) Dependence of the average speed of the Au/Pt (a) and Au/Pt−CNT (b) nanomotors upon the hydrogen peroxide concentration. A CNT loading of 0.50 mg/ml was used for preparing the Pt−CNT segment. *Y* error bars show the error limit at a 90% confidence interval.

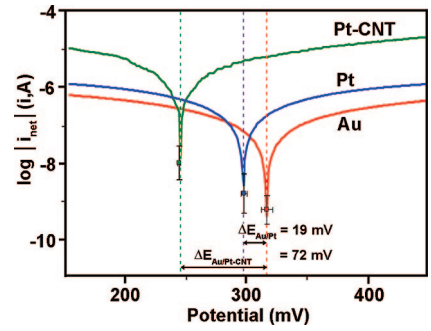

Figure 3. Electrode potentials of Au, Pt, and Pt−CNT. Tafel plots for Au (red), Pt (blue), and Pt-CNT (green) electrodes in a 5 wt % H_2O_2 solution. Dots below each Tafel plot denote the average of the mixed potential and log $|i_{net}|$ obtained from repeated scans, respectively. *X* and *Y* error bars represent the standard deviation. Differences in the mixed potentials are indicated as $\Delta E_{Au/Pt}$ and $\Delta E_{Au/Pt\text{-}CNT}$.

later, with open-circuit potential and Tafel-plot measurements, that the incorporation of CNT into the oxidative Pt side of the nanomotor has a dramatic effect upon the net oxidation of H_2O_2.

The CNT-enhanced electron-transfer reaction of the H_2O_2 fuel is exploited here for accelerating the speed of bimetal nanowire motors. Figure 2, top, illustrates that the amount of CNT loaded into the oxidative platinum end has a profound effect upon the speed of the catalytic nanomotors. The average speed (in 5 wt % H_2O_2) increases dramatically from 7.2 μm/s (a) to 28.7 μm/s (b) and 42.8 μm/s (c) upon raising the CNT loading in the Pt-plating solution from 0 to 0.25 and 0.50 mg/ml, respectively. Higher CNT concentrations [*e.g.*, 1.00 mg/ml (d)] do not offer additional speed enhancement. Such high CNT loading displayed greater irreproducibility due to incomplete suspension and aggregation of CNT in the growth solution that affect the CNT loading within the Pt segment during the electrodeposition.

Various control experiments were conducted. For example, since a Nafion-NBD solution was used for dispersing the CNT[14,20,21] we examined the role of Nafion-NBD (in the plating solution) in the absence of CNT. Only a slight speed enhancement (from 7.2 to 12.5 μm/s) was observed in the presence of Nafion-NBD (using 5 wt % H_2O_2), as compared to the dramatic increase from 7.2 to 42.8 μm/s observed in the presence of Nafion-NBD-CNT (0.5 mg/ml). In another control experiment we evaluated the role of Fe_3O_4 nanoparticles (often present as impurities in CNT) and their codeposition with Pt (at 0.50 mg/ml loading) on the motion of the nanomotor. The average velocity of the resulting Au/Pt−Fe_3O_4 nanomotors in 5 wt % hydrogen peroxide was 12.9 μm/s, that is, slightly higher than that of Au/Pt nanomotors but substantially smaller when compared to Au/Pt−CNT nanomotors (42.8 μm/s; not shown). These control experiments indicate that both Nafion-NBD and Fe_3O_4 have minimal effect upon the speed of the Au/Pt nanomotors and that the presence of CNT is crucial for the observed acceleration.

The concentration of the hydrogen peroxide fuel strongly influences the speed of the catalytic nanomotors (Figure 2, bottom). In accordance with earlier studies,[5] the average speed of the Au/Pt nanowires increases from 3.3 (in pure water) to 8.8 μm/s upon raising the H_2O_2 concentration to 10 wt % and decreases slightly at 15 wt % (a). In contrast, the average speed of the Au/Pt−CNT nanomotors increases rapidly from 3.3 to 42.8 μm/s upon raising the peroxide level to 5 wt % and then more slowly, reaching their highest speed of 51.0 μm/s at 15 wt % (b). These data imply that increasing the peroxide concentration from 0 to 15 wt% results in *ca.* 2 and 15-fold speed acceleration of the Au/Pt and Au/Pt−CNT nanomotors, respectively. The greatly increased speed of the Au/Pt−CNT nanomotors over the entire range (0−15 wt %) of H_2O_2 fuel indicates a substantial enhancement of the fuel consumption rate and reflects the high electrocatalytic activity of CNT toward H_2O_2 oxidation. The well-defined dependence of the speed of the Au/Pt−CNT nanowires upon the fuel concentration can form the basis for chemical sensing applications of catalytic nanomotors and for creating speed-controlled traffic zones.

Earlier work demonstrated that the speed of bimetallic nanowire motors is proportional to the mixed potential difference (ΔE) of the fuel at the corresponding metal segments.[11] The ΔE can be obtained from the Tafel plots of the anodic and cathodic reactions on the corresponding electrode materials. Figure 3 displays Tafel plots for Au, Pt, and Pt−CNT electrodes in a 5 wt

TABLE 1. Summary of the Mixed Potential, Open Circuit Voltage, and Exchange Current Density Obtained from the Electrochemical Potential Measurements

	electrochemical methods		
	tafel plot		
electrode	mixed potential[a] (mV)	current density (mA/cm^2)	open circuit potential[b] (mV)
gold	316 ± 5	0.48×10^{-3}	347 ± 3
platinum	297 ± 3	1.05×10^{-2}	289 ± 2
platinum−CNT	244 ± 1	4.71×10^{-2}	242 ± 3

[a]The mixed potential defined as potential at which the net current is zero. [b]The open circuit voltage is reported with respect to Ag/AgCl (3 M KCl) reference electrode.

% H_2O_2 solution. Considering the self-electrophoresis mechanism,[10] each metal segment behaves as an electrode (anode or cathode) in the galvanic cell. Tafel plots for Au, Pt, and Pt−CNT electrodes, shown in Figure 3, were obtained by plotting log $|i_{net}|$ *vs* potential. The mixed potential (dotted lines) represents the potential at which the net current (i_{net}) is zero.[23,24] In the case of nanomotors the redox reactive metals are connected, therefore the difference between the mixed potentials of the two metals determines the strength of the locally generated electric field and hence the rate of electron transfer and speed of the nanomotors.[11]

As summarized in Table 1, the potentials of the Au and Pt electrodes measured with two different electrochemical methods are positively shifted from the values reported by Mallouk *et al.*[11] However, the sequence of the mixed potentials and of the open-circuit voltages is in good agreement with the earlier report. Gold has a positive mixed potential of 19 mV with respect to Pt ($\Delta E_{Au/Pt}$) in 5 wt % H_2O_2, while the Au and Pt−CNT electrodes display a much larger mixed potential difference of +72 mV ($\Delta E_{Au/Pt\text{-}CNT}$). The dramatic speed acceleration of the Au/Pt−CNT nanomotors reflects this significantly larger ΔE of the Au and Pt−CNT electrode system. Cathodic reactions are thus expected to occur on the Au end, while anodic reactions proceed on either the Pt or Pt−CNT end of nanomotors. Since the Pt−CNT electrode has a lower mixed potential (244 mV) compared to the Pt one (297 mV), H_2O_2 is more easily oxidized at the Pt−CNT segment, leading to a faster reaction rate and an increased electron transfer inside the nanomotors. As indicated from Table 1, the Pt−CNT surface also displays a larger current density (4.71×10^{-2} mA/cm^2) compared to the Pt one (1.05×10^{-2} mA/cm^2), reflecting its enhanced electron-transfer process.

While all early experiments were conducted in the presence of the hydrogen peroxide fuel, we observed (toward the completion of this study) that changing the fuel composition through the addition of hydrazine to the peroxide solution leads to a dramatic speed acceleration of the Au/Pt−CNT nanowire motors. For example, Figure 4 illustrates motion traces of three representative nanomotors in the presence of 2.5 wt % H_2O_2 (a) and in a 2.5 wt % H_2O_2 solution containing 0.15 wt % hydrazine (b). The nanomotors travel (during this 4 s period) substantially longer distances in the presence of hydrazine (average distance of 373 μm versus 77 μm without the hydrazine), reflecting their faster movement in the mixed fuel solution. The traveling routes of Au/Pt−CNT nanomotors in this fuel appear to be mostly circular in nature with varying radii. Average speeds of 19.4 μm/s and 93.3 μm/s have thus been estimated in the peroxide and peroxide−hydrazine media, respectively (inset bar graph, Figure 4c). The former is in good agreement with the speed of CNT-loaded nanomotors in 2.5% hydrogen peroxide (Figure 2, bottom). It should be pointed out that about 4% of the nanowires display speeds higher than 200 μm/s in the mixed H_2O_2−hydrazine medium (Figure 4c, histrogram). This corresponds to over 100 body-lengths/second and exceeds the speed of most biomotors. The

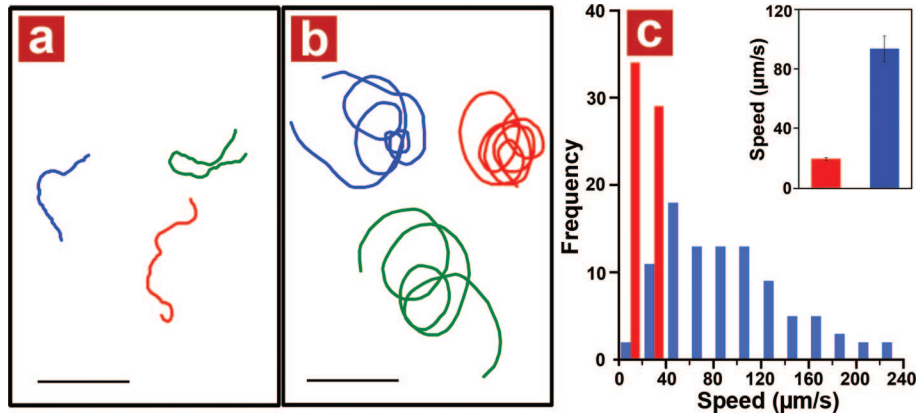

Figure 4. Hydrazine addition effects on CNT nanomotors. (a, b) Tracking lines illustrating a typical motion and moving distances of Au/Pt–CNT (0.50 mg/ml) nanomotors during a period of 4 s in the presence of 2.5 wt % hydrogen peroxide fuel, without (a) and with (b) the addition of 0.15 wt % hydrazine. Scale bar is 50 μm. (c) Histograms of the speed distribution of the Au/Pt–CNT nanomotors without (red) and with (blue) hydrazine (in the 2.5 wt % hydrogen-peroxide fuel solution) measured from the movement of the nanomotors over a 10 s period. Bar graph with *Y* error bars (inset) represents the mean of average speeds (μm/s) and the error limit at 90% confidence interval of the corresponding nanomotors, respectively.

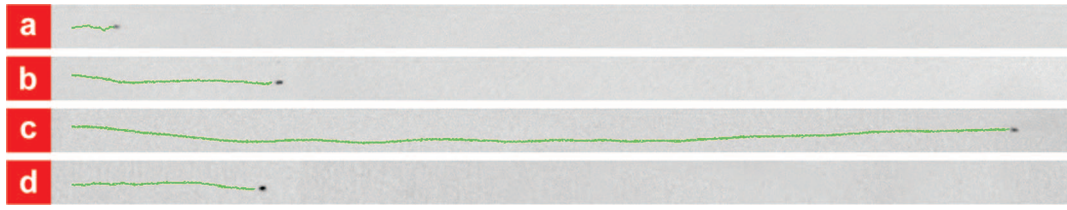

Figure 5. Nanomotor racing. Optical images, superimposed with tracked lines, illustrating the speed of the Au/Ni/Au/Pt (a, d) and Au/Ni/Au/Pt−CNT (b, c) nanomotors, under an applied (weak) magnetic field and 2.5 wt % hydrogen peroxide, with (c, d) and without (a, b) 0.15 wt % hydrazine. A CNT loading of 0.50 mg/ml was used for preparing the Pt−CNT segment.

Ⓦ video 2, showing nanomotor "racing" is available.

dramatic acceleration in the mixed fuel is attributed to a hydrazine-induced enhancement of the catalytic reductions of both oxygen[25] and hydrogen peroxide[26] at the cathodic gold segment, as well as to the efficient catalytic decomposition of hydrazine in the presence of a catalytic carbon surface and hydrogen peroxide.[27] Even though hydrazine has previously been used, recently as a fuel for a Au/Pd bimetallic fluid pumping system,[28] this represents the first report of a dramatic speed acceleration due to a mixed fuel solution.

The magnetic alignment of nickel-containing nanowires[6] permits "racing" of different nanomotors in a straight line under a weak magnetic field. Figure 5 displays a comparison of the displacement of four nanomotors (during a 4 s period; captured from video 2) in connection to four nanowire/fuel compositions: Au/Ni/Au/Pt nanomotor in 2.5 wt % H_2O_2 (a), Au/Ni/Au/Pt−CNT nanomotor in 2.5 wt % H_2O_2 (b), Au/Ni/Au/Pt−CNT nanomotor in mixed H_2O_2 (2.5 wt %)−hydrazine (0.15 wt %) (c), and Au/Ni/Au/Pt nanomotor in mixed H_2O_2 (2.5 wt %)−hydrazine (0.15 wt %) (d). An AVI movie, video 2, available with Figure 5, shows the corresponding real time side-by-side race between the Au/Ni/Au/Pt and Au/Ni/Au/Pt−CNT nanomotors in an aqueous H_2O_2 solution with and without hydrazine. This movie illustrates a remarkable (~20-fold) speed acceleration—from 5.0 (a) to 94.0 (c) μm/s—by combining the CNT and hydrazine additions (to the motor and fuel, respectively). The short displacement of the Au/Ni/Au/Pt nanomotor in the mixed fuel, compared with the 5-fold displacement of the Au/Ni/Au/Pt−CNT nanomotor in the same fuel (72 (d)−376 (c) μm, respectively), supports that the presence of CNT in the nanomotor is crucial for efficient conversion of the mixed fuel to mechanical energy. As indicated by the green trace lines, the directionality of the nanomotors is controllable even at the very high speeds of the Au/Ni/Au/Pt−CNT nanomotor. It is important to note that further increase in speed could be realized by fine-tuning the concentration and ratio of mixed fuels.

Such higher energy conversion can be enumerated by comparing the output power of different nanomotors in different fuels. The data summarized in Table 2 shows the ratio of the output power[10] of Au/Ni/Au/Pt−CNT nanomotors to those of Au/Ni/Au/Pt nanomotors in the same and in different fuels. In the 2.5 wt % H_2O_2 fuel, the output power of Au/Ni/Au/Pt−CNT nanomotors is about 12 times greater than that of Au/Ni/Au/Pt nanomotors (Figure 5b *vs* 5a). The output power ratio of Au/Ni/Au/Pt−CNT to Au/Ni/Au/Pt nanomotors (Figure 5c *vs* 5d) is increased further to 27 in the presence of the mixed fuel (2.5 wt % H_2O_2−0.15 wt % hydrazine). With the addition of both CNT and hydrazine (to the nanowire and fuel, respectively), the new nanomotor system exhibits an outstanding performance that is over 350 times more powerful than that of common Au/Ni/Au/Pt nanomotors in H_2O_2 fuel (Figure 5c *vs* 5a).

In conclusion, we have demonstrated a dramatic acceleration of self-powered bimetal nanomotors based on the incorporation of CNT into the Pt segment of Au/Pt nanowires. Such CNT-induced acceleration of catalytic nanomotors reflects the enhanced oxidation of the hydrogen peroxide fuel. We also illustrated that the speed of nanomotors can be further increased upon adding hydrazine to the peroxide fuel and that this efficient movement can be manipulated magnetically. Current studies in our laboratory aim at understanding the underlying mechanisms and forces involved in these accelerated nanomotors and exploring new energy-rich chemical reactions (based on different choices of fuels and a variety of motor compositions). For example, recent experiments indicate a similar acceleration upon doping the CNT into a palladium

TABLE 2. Summary of the Output Power Ratio of Au/Ni/Au/Pt−CNT to Au/Ni/Au/Pt Nanomotors in the H_2O_2 or Mixed H_2O_2−Hydrazine Fuels

$fuel_1/fuel_2$	$(nanomotor_1)/(nanomotor_2)$	output power ratio[a]
2.5 wt % H_2O_2/2.5 wt % H_2O_2	(Au/Ni/Au/Pt−CNT)/(Au/Ni/Au/Pt)	12.0
2.5 wt % H_2O_2−0.15 wt % hydrazine/2.5 wt % H_2O_2−0.15 wt % hydrazine	(Au/Ni/Au/Pt−CNT)/(Au/Ni/A u/Pt)	27.3
2.5 wt % H_2O_2−0.15 wt % hydrazine/2.5 wt % H_2O_2	(Au/Ni/Au/Pt−CNT)/(Au/Ni/Au/Pt)	353.4

[a]The output power ratio ($P_{O(1)}/P_{O(2)}$) is calculated from the output power of nanomotor-fuel system 1 to those of nanomotor-fuel system 2. Output power is the product of the nanomotor velocity and drag force generated as the nanomotors move through the fuel solution.[10]

(anodic) segment instead of a platinum one (not shown). We expect that these studies will lead to even more energy-efficient nanomotors and will open up new opportunities for nanoscale vehicle systems. Such high-performance nanomotors should allow transport and release of "heavy" loads, locomotion in physiological conditions, and the design of more sophisticated nanosystems performing multiple complex tasks. Preliminary data indicate that the new CNT-doped nanomotors are still self-motile when loaded with particles having diameters of 3 μm (*i.e.*, >10-fold larger than their diameter) and alternately in salt solutions where common Au/Pt nanomotors do not move. Controlled motion in microfluidic channels is also being accomplished and will be reported separately. We are also designing nanomotor-based sensing systems for monitoring the levels of fuels, including the biosensing of glucose (based on the direct speed-concentration correlation).

METHODS

Purification of Multiwalled Carbon Nanotubes (CNT). CNT, obtained from NanoLab (catalog no. PD30L5-20, Newton, MA), were purified in accordance to the previously reported procedure.[14] In brief, 100 mg of CNT were dispersed in 100 mL of concentrated nitric acid and sonicated at 60 °C for 90 min. The solution was then incubated at 60 °C overnight. Following the acid treatment the CNT suspension was centrifuged at 3000 rpm for 30 min to separate the CNT from the acid solution. The acid treated CNT were washed repeatedly with nanopure water (18.2 MΩU) until the solution pH was neutral. Finally, the purified CNT were dried at 60 °C until a constant mass was obtained. All CNT containing solutions were sonicated for 2 h prior to use.

Synthesis and Characterization of Catalytic Nanomotors. The bisegment nanomotors were prepared by electrodepositing the corresponding metals or hybrid metal-CNT into a porous alumina membrane template (catalog no. 6809-6022; Whatman, Maidstone, U.K.). The length (~1 μm) of each nanomotor segment was obtained by controlling the electrodeposition charge, while its diameter (~220 nm) was predetermined by the pore size of the membrane. A thin gold film was first sputtered on the branched side of the membrane to serve as a working electrode. The membrane was assembled in a plating cell with aluminum foil serving as an electrical contact for the subsequent electrodeposition. To synthesize well-shaped cylindrical nanomotors, a sacrificial silver layer was electrodeposited into the branched area (~1−2 μm thickness) of the membrane using a silver plating solution (1025 RTU@4.5 Troy/Gallon; Technic Inc., Anaheim, CA) and a total charge of 2 coulombs (C) at −0.9 V (*vs* Ag/AgCl, in connection to a Pt wire counter electrode). This was followed by an electrodeposition of gold (1.5 C) from a gold-plating solution (Orotemp 24 RTU RACK; Technic Inc.) at −0.9 V (*vs* Ag/AgCl). Subsequently, platinum or platinum−CNT were deposited galvanostatically at −2 mA for 50 min from a platinum-plating solution (Platinum RTP; Technic Inc.) or using a platinum-plating solution containing various amounts (0.25−1.00 mg/ml) of CNT, along with 0.1 wt% Nafion and 2 mM 4-nitrobenzenediazonium tetrafluoroborate (NBD), respectively. The procedure used to prepare the Pt−CNT solid segment was adapted from previously reported methods for the plating of Pt−CNT composites.[20,21] Such protocol ensures uniform dispersion of CNT in the plating solution and hence a homogeneous loading of CNT within the Pt segment. This synthesis resulted in bisegment nanomotors where each segment is ~1 μm in length. The Au/Pt−Fe_3O_4 nanowires (tested in control experiments) were prepared by depositing the Pt−Fe_3O_4 segment galvanostatically using the same conditions as for the Pt and Pt−CNT segments, from a platinum plating solution containing a suspension of Fe_3O_4−$(C_9H_{19}COOH)_2$ nanoparticles (0.5 mg/ml). The bilayer surfactant-coated iron oxide [Fe_3O_4−$(C_9H_{19}COOH)_2$] nanoparticles were synthesized according to a previously reported procedure,[22] except that at the final step the nanoparticles were washed thoroughly with deionized water and dried at 100 °C. Nickel-containing nanomotors (Au/Ni/Au/Pt and Au/Ni/Au/Pt−CNT) were synthesized for the magnetically controlled experiments. Following the plating of the first gold segment (0.75 C), nickel was electrodeposited from a nickel plating solution [20 g L^{-1} $NiCl_2 \cdot 6H_2O$, 515 g L^{-1} $Ni(H_2NSO_3)_2 \cdot 4H_2O$, and 20 g L^{-1} H_3BO_3 (buffered to pH 3.4)] at −1.0 V (*vs* Ag/AgCl). A total charge of 0.5 and 2.0 C was used for plating nickel for the "racing" nanomotors (of Figure 5) and the speed-controlled nanomotors (of Figure 4), respectively. The second gold segment (0.75 C) was then deposited, followed by the growth of the Pt or Pt−CNT segment, as previously described. After depositing the nanomotors, the membrane was removed from the plating cell and rinsed thoroughly with nanopure water to remove all residues. The sputtered gold layer and the silver layer were simultaneously removed by mechanical polishing using cotton tip applicators soaked with 35% HNO_3 for *ca.* 5 min to ensure complete silver dissolution. The bisegment nanowires were then released by immersing the membrane in 3 M NaOH for 30 min. These nanowires were collected by centrifugation at 10 000 rpm for 5 min and washed repeatedly with nanopure water (18.2 $M\Omega \cdot cm^{-1}$) until a neutral pH was achieved. Between washing steps the nanowire solution was mixed and briefly sonicated (several seconds) to ensure the complete dispersion of nanowires in the washing water and hence the removal of salt residuals entrapped in the nanowire aggregate after centrifugation. Special attention was paid to the nanowires being washed directly before testing and suspended in freshly obtained nanopure water because of significant deceleration of the nanomotors speed in the presence of salt ions. All nanomotor solutions were stored in nanopure water at room temperature and their speed tested within a day of synthesis. The nanowires were characterized using an FEI XL30 scanning electron microscope (SEM; FEI Co., Hillsboro, OR). The SEM images were used to determine the length of each segment of the nanomotors.

Tracking of Nanomotors Movement. The nanomotor suspension in nanopure water was first diluted to obtain a concentration of ~2.6×10^6 nanomotors/ml. A 10 μl portion of the diluted nanomotor suspension was then mixed with 10 μl of different concentrations (5−30 wt %) of the hydrogen peroxide fuel solution. This mixing resulted in the final nanomotor/aqueous hydrogen peroxide solution where both original constituents were diluted by half. In the case of the mixed fuel, a mixture containing 5.0 wt % hydrogen peroxide and 0.3 wt % hydrazine solutions was freshly prepared and mixed with the nanowire suspension using a 1:1 volume ratio. The final solution was then transferred *via* capillary action to a capillary microslide (0.1 mm thickness, 2 mm width, and 50 mm length; VitroCom Inc., Mountain Lakes, NJ). The real-time movement of the nanomotors in the hydrogen peroxide solution was observed and recorded (starting ~5 min after the preparation of the final solution), at 200× total magnification, using an optical microscope (Nikon Instrument Inc., Eclipse80i, Melville, NY) equipped with a Photometrics CoolSnap CF camera (Roper Scientific, Duluth, GA) and a MetaMorph 7 software (Molecular Devices, Sunnyvale, CA). Movies were acquired over 10 s at a frame rate of 10 frames/second. Usually 5 movies were recorded along the length of the capillary microslide to ensure accurate population sampling. The speed of the nanomotors was measured using MetaMorph 7's tracking software which determined the position of the nanomotor in each frame, calculated the displacement distances between the frames, and in turn the average velocity of each nanomotor. For each type of nanomotor, more than 50 nanomotors were tracked to obtain a reliable average speed (and the error limit at a 90%

confidence interval), representative of the overall sample. Grubbs' test was used to detect outliers in a data set at 95% confidence level ($\alpha = 0.05$).

For the magnetically aligned racing nanomotors, a 9.5 mm cube-shaped Neodymium (NdFeB) magnet (1.32 T from K&J Magnetics Inc., Jamison, PA) was fixed to a custom magnet holder and attached directly to the microscope condenser stage at *ca.* 10 mm below from the microcapillary tube (containing the nanowires). The magnetic pole (from north to south) of the magnets was perpendicular to the optical axis of the microscope. This position of the magnet allowed for a weak parallel magnetic field on the microcapillary tube.

Electrochemical Measurements. Two electrochemical methods, Tafel plots and open circuit potentials, were used to obtain the potential established at each nanomotor segment (Au, Pt, and Pt−CNT) in a hydrogen peroxide environment. The first method (Tafel plots) measures the mixed potential which represents an intermediate of equilibrium potentials of the electrode on which several reactions occur simultaneously.[24] Gold, platinum, and glassy carbon (GC) disk electrodes (diameter of 2, 2, and 3 mm, respectively) were obtained from CH Instrument Inc. (Austin, TX). Platinum−CNT was co-deposited on the GC electrode from a platinum plating solution containing 0.5 mg/ml CNT using the same conditions as those used for growing the nanowires (with the exception of a 10 min deposition). Gold, platinum, and platinum−CNT coated GC disk electrodes were used as the working electrode in the electrochemical potential measurements. Cyclic voltammetry of 5 wt % aqueous hydrogen peroxide (without any electrolyte) was performed using the CH Instrument Model CHI630C at a scan rate of 50 mV/s and over a potential range of 0.2 to 0.8 V (*vs* Ag/AgCl, 3 M KCl reference), along with a glassy carbon counter electrode. A summation of the anodic (i_a) and cathodic (i_c) currents at each applied potential was calculated, resulting in the net current (i_{net}). The mixed potential, at which the anodic and cathodic currents are equal (*i.e.*, zero net current), was obtained by extrapolating the linear Tafel regime of the plot of log $|i_{net}|$ *versus* potential.[23] The second method (open circuit potentials) measures the electrode potential with respect to a Ag/AgCl (3 M KCl) reference electrode at zero current, which is the open circuit voltage (OCV). Zero-current potentiometry was performed using 5 wt % H_2O_2 as a liquid conductor. The stabilizing potential was identified as the electrode potential (*vs* Ag/AgCl, 3 M KCl) in the presence of 5 wt % H_2O_2.

Acknowledgment. This work was supported by the National Science Foundation (Grant No. CHE 0506529). R. Laocharoensuk acknowledges a fellowship from the DPST Program, Thailand.

REFERENCES AND NOTES

1. Akin, D.; Sturgis, J.; Ragheb, K.; Sherman, D.; Burkholder, K.; Robinson, J. P.; Bhunia, A. K.; Mohammed, S.; Bashir, R. Bacteria-Mediated Delivery of Nanoparticles and Cargo into Cells. *Nat. Nanotechnol.* **2007**, *2*, 441–449.
2. van den Heuvel, M. G. L.; Dekker, C. Motor Proteins at Work for Nanotechnology. *Science* **2007**, *317*, 333–336.
3. Clemmens, J.; Hess, H.; Doot, R.; Matzke, C. M.; Bachand, G. D.; Vogel, V. Motor-Protein "Roundabouts": Microtubules Moving on Kinesin-Coated Tracks through Engineered Networks. *Lab Chip* **2004**, *4*, 83–86.
4. Ismagilov, R. F.; Schwartz, A.; Bowden, N.; Whitesides, G. M. Autonomous Movement and Self-Assembly. *Angew. Chem., Int. Ed.* **2002**, *41*, 652–654.
5. Paxton, W. F.; Kistler, K. C.; Olmeda, C. C.; Sen, A.; St.Angelo, S. K.; Cao, Y.; Mallouk, T. E.; Lammert, P. E.; Crespi, V. H. Catalytic Nanomotors: Autonomous Movement of Striped Nanorods. *J. Am. Chem. Soc.* **2004**, *126*, 13424–13431.
6. Kline, T. R.; Paxton, W. F.; Mallouk, T. E.; Sen, A. Catalytic Nanomotors: Remote-Controlled Autonomous Movement of Striped Metallic Nanorods. *Angew. Chem., Int. Ed.* **2005**, *44*, 744–746.
7. Fournier-Bidoz, S.; Arsenault, A. C.; Manners, I.; Ozin, G. A. Synthetic Self-Propelled Nanorotors. *Chem. Commun.* **2005**, 441–443.
8. Fennimore, A. M.; Yuzvinsky, T. D.; Han,Wei-Qiang; Fuhrer, M. S.; Cumings, J.; Zettl, A. Rotational Actuators Based on Carbon Nanotubes. *Nat. Mater.* **2003**, *424*, 408–410.
9. Regan, B. C.; Aloni, S.; Ritchie, R. O.; Dahmen, U.; Zettl, A. Carbon Nanotubes as Nanoscale Mass Conveyors. *Nature* **2004**, *428*, 924–927.
10. Paxton, W. F.; Sen, A.; Mallouk, T. E. Motility of Catalytic Nanoparticles through Self-Generated Forces. *Chem.—Eur. J.* **2005**, *11*, 6462–6470.
11. Wang, Y.; Hernandez, R. M.; Bartlett, D. J.; Bingham, J. M.; Kline, T. R.; Sen, A.; Mallouk, T. E. Bipolar Electrochemical Mechanism for the Propulsion of Catalytic Nanomotors in Hydrogen Peroxide Solutions. *Langmuir* **2006**, *22*, 10451–10456.
12. Kim, S. N.; Rusling, J. F.; Papadimitrakopoulos, F. Carbon Nanotubes for Electronic and Electrochemical Detection of Biomolecules. *Adv. Mater.* **2007**, *19*, 3214–3228.
13. Wang, J. Carbon-Nanotube Based Electrochemical Biosensors: A Review. *Electroanalysis* **2005**, *17*, 7–14.
14. Wang, J.; Musameh, M.; Lin, Y. Solubilization of Carbon Nanotubes by Nafion toward the Preparation of Amperometric Biosensors. *J. Am. Chem. Soc.* **2003**, *125*, 2408–2409.
15. Qu, F.; Yang, M.; Shen, G.; Yu, R. Electrochemical Biosensing Utilizing Synergic Action of Carbon Nanotubes and Platinum Nanowires Prepared by Template Synthesis. *Biosens. Bioelectron.* **2007**, *22*, 1749–1755.
16. Chen, Z.; Waje, M.; Li, W.; Yan, Y. Supportless Pt and PtPd Nanotubes as Electrocatalysts for Oxygen-Reduction Reactions. *Angew. Chem., Int. Ed.* **2007**, *46*, 4060–4063.
17. Kurusu, F.; Tsunoda, H.; Saito, A.; Tomita, A.; Kadota, A.; Kayahara, N.; Karube, I.; Gotoh, M. The Advantage of Using Carbon Nanotubes Compared with Edge Plane Pyrolytic Graphite as an Electrode Material for Oxidase-Based Biosensors. *Analyst* **2006**, *131*, 1292–1298.
18. Gao, L.; Zhuang, J.; Nie, L.; Zhang, J.; Zhang, Y.; Gu, N.; Wang, T.; Feng, J.; Yang, D.; Perrett, S. Intrinsic Peroxidase-Like Activity of Ferromagnetic Nanoparticles. *Nat. Nanotechnol.* **2007**, *2*, 577–583.
19. Kongkanand, A.; Kuwabata, S.; Girishkumar, G.; Kamat, P. Single-Wall Carbon Nanotubes Supported Platinum Nanoparticles with Improved Electrocatalytic Activity for Oxygen Reduction Reaction. *Langmuir* **2006**, *22*, 2392–2396.
20. Guo, D. -J.; Li, H. L. High Dispersion and Electrocatalytic Properties of Platinum on Functional Multi-Walled Carbon Nanotubes. *Electroanalysis* **2005**, *17*, 869–872.
21. Cui, G.; Zhi, L.; Thomas, A.; Kolb, U.; Lieberwirth, I.; Müllen, K. One-Dimensional Porous Carbon/Platinum Composites for Nanoscale Electrodes. *Angew. Chem., Int. Ed.* **2007**, *46*, 3464–3467.
22. Shen, L.; Laibinis, P. E.; Hatton, T. A. Bilayer Surfactant Stabilized Magnetic Fluids: Synthesis and Interactions at Interfaces. *Langmuir* **1999**, *15*, 447–453.
23. Bard, A. J.; Faulkner, L. R. *Electrochemical Method: Fundamentals and Applications*; John Wiley & Sons, Inc.: New York, 2000.
24. Bagotsky, V. S. *Fundamentals of Electrochemistry*, 2nd ed.; John Wiley & Sons, Inc.: New York, 2005.
25. Moon, J. -S.; Park, K. -K.; Kim, J. -H.; Seo, G. The Reduction Reaction of Dissolved Oxygen in Water by Hydrazine over Platinum Catalyst Supported on Activated Carbon Fiber. *Appl. Catal. A* **1999**, *184*, 41–48.
26. Shankaran, D. R.; Shim, Y. B. An Amperometric Sensor for Hydrogen Peroxide Based on a (3-Mercaptopropyl)trimethoxysilane Self-Assembled Layer Containing Hydrazine. *Electroanalysis* **2002**, *14*, 704–707.
27. Ishida, K.; Nagase, M.; Uetake, N.; Anazawa, K.; Nakamura, F.; Aizawa, M.; YoshikaWA, H. Low Corrosive Chemical Decontamination Method Using pH Control, (II) Decomposition of Reducing Agent by Using Catalyst with Hydrogen Peroxide. *J. Nucl. Sci. Technol.* **2002**, *39*, 941–949.
28. Ibele, M. E.; Wang, Y.; Kline, T. R.; Mallouk, T. E.; Sen, A. Hydrazine Fuels for Bimetallic Catalytic Microfluidic Pumping. *J. Am. Chem. Soc.* **2007**, *129*, 7762–7763.